Electrical and microstructural properties of silver thin films

Shiva L. U*, N. H. Ayachit, Udachan L. A

Department of Physics, Rani Channamma University, Belagavi-591 156, Karnataka, India. Channabasaveshwar Post Graduate Studies & Research Centre, Bhalki , Dist: Bidar, Karnataka, India.

*Corresponding author e-mail : shivaudachan8@gmail.com

Abstract

The growth, structure and electrical properties of evaporated thin silver (Ag) films have been an object of very extensive investigation over the years as it has the highest electrical conductivity among all metals. The Ag thin films have been studied by thermal evaporation on glass, mica and Teflon. The thickness of Ag films in this investigation is in the range of 10 - 150 nm. The electrical properties include measurement of resistivity, temperature coefficient of resistance (TCR) and activation energy (E_a) as a function of film thickness (t), have been studied. The experimental results are analyzed in the light of Fuchs-Sondheimer (FS) and Mayadas-Shatzkes (MS) theories. The resistivity of infinitely thick Ag film and TCR are found to be 3.53 x 10^{-8} Ω m and 3.73 x 10^{-3}/ ^{0} C, respectively. The mean free path of conduction electron calculated from the resistivity and TCR data are 42.8 nm and 26.28 nm, respectively. A study on the initial stages of growth of Ag films and the microstructural properties have also been undertaken by using Scanning Electron Microscope (SEM) for films grown on different substrates and for different thicknesses.

Keywords: Thin silver films, electrical resistivity, electron mean free path, TCR and microstructural properties.

1. Introduction:

Ag is an extremely soft, ductile and malleable transition metal, though it is slightly less malleable than gold. Ag has a brilliant white metallic luster that can take a high polish. Very high electrical and thermal conductivity is common to the elements in group 11, because their single *s* electron is free and does not interact with the filled *d* sub shell, as such interactions involve lower electron mobility.

Ag is the most commonly used material for many applications, since showing the highest conductivity and most reflecting. Films have to be very thin, in order to preserve transparency in the visible. New applications of transparent conductive thin films have recently been developed, leading to what is known as transparent electronics, used for flat displays, flat light sources, photovoltaic cells and smart windows. An alternative to the use of traditional transparent conductive oxides (TCO), such as indium-tin oxide (ITO). The Saint-Gobain

solution makes use of very thin films of Ag [1]. This should bring an important advantage, because Ag is cheaper than that of indium and its sourcing is more durable.

Ag is one of the best conducting metals and is widely used in the modern world for electrical conduction in multiple industries and applications, including light-emitting diodes (LED), organic light emitting diodes (OLED) and flat-panel displays (FPD) [2], antireflection coatings [3], gas sensors [4] and as contact electrodes in solar cells [5]. Ag is used as contact metallization in the microelectronic devices due to its low surface resistivity ($1.57 \times 10^{-8}\,\Omega$ m at room temperature) [6] and its thermal stability.

Ag thin films have also been widely applied in optical applications, mainly due to their high transparency and neutral color in the visible range. They also exhibit extremely high reflectivity in the near infrared (IR) and IR parts of the spectrum. These properties make Ag thin films as ideal candidates for low-thermal-emissivity (Low-E) coatings on glass panels, leading to energy-efficient windows for residential and commercial buildings, ultimately leading to substantial energy savings [2]. In general, the desired properties for Ag films used as metallization contacts are as follows: low specific resistivity, good thermal stability, high uniformity across the flat substrate, low particle contamination, good adherence to substrate, low manufacturing costs and Ag has unique optical properties for topical applications such as plasmonics. The adaptive property of Ag films has been studied and employed for protein sensing with surface-enhanced Raman scattering (SERS)[7].

In applications where electrical and optical properties are important, precise measurement of thickness is required as it dictates the structure (micro/nano). Thickness of films can alter properties such as resistivity, capacitance, durability optical wave-length, reflectivity and opacity.

In view of the above said interesting properties of Ag, it is desirable to study its electrical and microstructural properties in the thin film form, as the micro-structure and film thickness govern physical properties of thin films. Thin films of Ag have been grown in a conventional vacuum coating unit in the thickness range of 50 -150 nm. The electrical measurements have been done in-situ by the standard four probe technique. Microstructural analysis of Ag films has also been undertaken.

International Journal of Nanoelectronics and Materials

In Press, Accepted Manuscript – Note to users

UNIVERSITI
MALAYSIA
PERLIS
UniMAP

2. Theoretical Study:

(2.1) Electrical conductivity and Electron mean free path(l) in bulk Ag:

A theory of metallic conductivity based on average velocity was developed by Drude in 1900. Lorentz in 1905 reinvestigated the problem using Boltzmann statistics. However, the use of classical statistics led to serious difficulties. Then in 1928 Sommerfeld calculated the conductivities along the line of Lorentz theory by replacing the classical statistics with Fermi-Dirac statistics. Sommerfeld did not investigate the actual mechanism of interaction between electrons and lattice any further, but assumed that a relaxation time can be defined which is a function of energy of electrons only. He obtained an expression for electrical conductivity (σ) as [8] is given by,

$$\sigma = \frac{ne^2 \tau}{m} \tag{1}$$

where n is the concentration of electrons/m^3, e is the electronic charge, m is the mass of electron and τ is the relaxation time, which is given by $\frac{l}{V_F}$, where l is electron mean free path and V_F is velocity of electrons at the Fermi surface. It is interesting to note that although all electrons take part in the conduction mechanism but the relaxation time of electrons occurs at the Fermi level in conductivity.

The reason for selecting this thickness range of 50 - 150 nm is that we have first estimated the electron mean free path in bulk Ag by the electrical conductivity in equation (1) as 52.5 nm.

(2.2) Electrical Resistivity in thin films:

(a) Fuchs-Sondheimer(FS) theory:

The electrical response of metal thin films approaching the thickness in the range of electron mean free path is highly affected by the electronic scattering with interfaces and defects. Fuchs worked out the detailed analysis of the size effect by solving the Boltzmann's transport equation with appropriate boundary conditions. He obtained an expression for the electrical resistivity ratio [9] as,

$$\frac{\rho_0}{\rho} = \frac{\sigma}{\sigma_0} = 1 - \frac{3}{4}\left(\lambda - \frac{\lambda^3}{12}\right) E_i(-\lambda) - \frac{3}{8\lambda}\left(1 - e^{-\lambda}\right) - \left(\frac{5}{8} + \frac{\lambda}{16} - \frac{\lambda^2}{16}\right) e^{-\lambda}$$

Where

$$- E_i(-\lambda) = \int_\lambda^\infty \left(\frac{e^{-t}}{t}\right) dt \tag{2}$$

σ_0 is conductivity of an infinitely thick film, σ is the conductivity of thin film, $\lambda = t/l$, is the ratio of film thickness, t and conduction electron mean free path, l.

Equation 2 can be approximated for convenience as,

$$\rho = \rho_0 \left[1 + \frac{3}{8\lambda} \right], \quad \lambda > 0.1 \tag{3}$$

Where ρ and ρ_0 are electrical resistivity of the film and infinitely thick film. There is a good agreement of this equation with the exact equation (2) [9] over a wide range of λ.

However, this consideration is for total scattering. Therefore a sophisticated theory was developed by Sondheimer [10] to measure the deviation of size effect from the bulk behavior. He introduced a specularity parameter (p), which represents the fraction of electrons, which gets specularly scattered from the film surfaces. p has the value ranging from 0 to 1. For complete specular reflection $p = 1$, the conductivity is not thickness dependent in this case. For total diffuse scattering $p = 0$. Assuming a fraction p of electrons to be specularly scattered at the surface of the film and the remaining fraction getting scattered diffusely, equation (3) can be written as,

$$\rho = \rho_0 \left[1 + \frac{3(1-p)}{8\lambda} \right], \quad \lambda > 0.1 \tag{4}$$

This expression is known as Fuchs-Sondheimer equation and is extensively used to analyze experimental results. The second term on the right hand side (RHS) of equation (3) represents contribution to the total resistivity (ρ) based on the size effect.

(b) Mayadas-Shatzkes(MS) theory:

The Fuchs theoretical consideration did not explain the high resistivity observed in some of very thin metallic films. These thin films often have island or grain like structure and are discontinuous. When these grains or islands have the dimensions of the order of electron mean free path, the scattering at the grain boundaries is very high leading to a very high resistivity. In order to estimate the contribution of grain boundary scattering to the total film resistivity, Mayadas-Shatzkes [11] made the following assumptions.

In thin films the individual crystal grow roughly vertically from the substrate to the upper surface of the film, the grain boundaries need to be considered are those lying parallel and perpendicular to the applied field, the grain boundary potential could be represented by Dirac δ - function and the dimensions of the grains are approximately equal to the electron mean free path.

In this model, the simultaneous action of these electron scattering mechanisms was considered in order to calculate the total resistivity of the metallic films. They are isotropic background scattering, surface scattering and grain boundary scattering. Mayadas-

International Journal of Nanoelectronics and Materials

In Press, Accepted Manuscript – Note to users

UNIVERSITI
MALAYSIA
PERLIS

UniMAP

Shatzkes solved the Boltzmann's transport equation using the above model, imposing necessary boundary conditions and finally arrived at the relation.

$$\frac{\rho_0}{\rho_g} = 3[\frac{1}{3} - \frac{1}{2(\alpha')} + \alpha') \quad \text{for small } \alpha' \tag{5}$$

Where (ρ_o/ρ_g) is the ratio of resistivity back ground (ρ_o) to grain boundary resistivity ρ_g, and α' is the scattering power of grain boundaries and is given by,

$$\alpha' = \frac{l \; R'}{d \; (1-R')} \tag{6}$$

Where d is the grain diameter, and R' is the grain boundary reflection coefficient.

With the grain boundary scattering consideration, the total resistivity of the film becomes

$$\rho = \rho_0 \left[1 + \frac{3(1-p)}{8\lambda} + \frac{3}{2} \alpha' \; \right] \tag{7}$$

The third term on the right hand side (RHS) of equation (7) is the contribution to the total resistivity (ρ) from grain boundary scattering.

Numbers of models for the electrical resistivity of thin films are given by many investigators [2,12,13].

(2.3) Temperature Coefficient of Resistance-TCR(α):

Another important electrical parameter, the temperature coefficient of resistance (TCR), which is generally different in case of thin films from their bulk value. The temperature dependent part of resistivity arises from the interaction of phonons with electrons. The TCR (α_B) is defined for bulk metals as [14],

$$\alpha_B = \frac{1}{\rho_B} \quad \frac{d\rho_B}{dT} \tag{8}$$

Similarly for thin films, the TCR, α_t is given by

$$\alpha_t = \frac{1}{\rho_t} \quad \frac{d\rho_t}{dT} \tag{9}$$

and we may write

$$\alpha_t \rho_t = \alpha_B \rho_B = \rho_0 \alpha_0 = \text{constant, for } \lambda \gg 1 \tag{10}$$

This equation is an alternative form of Matthiessen's rule and is independent of p. For $\lambda \ll 1$, deviation from the Matthiessen's rule is expected for all values of $p < 1$, because of the size effect. Using conductivity or resistivity expression for the thin films (F-S model), the corresponding expression for TCR from equation (4).

$$\alpha_t = \alpha_0 \left[1 - \frac{3}{8\lambda} (1-p) \right], \quad \text{for } \lambda > 0.1 \tag{11}$$

where α_t is the TCR of thin film, α_0 is the TCR of infinitely thick film, p is the specularity parameter and λ is the ratio of film thickness(t) to the electron mean free path(l).

(2.4) Activation Energy(E_a):

For metallic films, the activation energy for the thermal process, by considering the variation of resistance (R'') with temperature (T) of film, is given by [15].

$$R'' = R_0 \ \exp\left[\frac{E_a}{KT}\right] \tag{12}$$

where R'' is the resistance of the film at temperature T (K), R_0 is the resistance of the film at 0 (K) and K is the Boltzmann's constant.

(2.5) Thickness dependence of microstructure and substrate materials in Ag thin films:

Nucleation and cluster formations from vapor phase will involve the condensation of vapor directly to the solid phase or via liquid phase on the surface of the substrates. The condensation of vapor atoms/molecules on an inert solid substrate takes place from a supersaturated condition of vapors. The details are discussed in the results and discussion in sub section (4.5) of section 4.

(2.6) Energy Dispersive Spectroscopy, EDS Analysis:

One of the most powerful attachments of SEM is Energy Dispersive X-ray Spectroscopy (EDS). Atomic qualitative and quantitative information from the specimen can be supplied by an EDS system and discussed in sub section 4.6 of section 4.

3. Experimental Technique:

3.1 Thermal evaporation in vacuum:

The vacuum coating unit used in the present investigation is the Hind High Vacuum Coating Unit, Model 12A4D", to grow thin films of Ag. The film thickness was controlled and measured by means of an in-built Quartz Crystal Digital Thickness Monitor (Model DTM-101). Ag of purity 99.99% was evaporated from a molybdenum boat at the rate of 0.5 nm/s under a vacuum of 2×10^{-6} Torr on to cleaned glass, mica and teflon substrates at room temperature($23\ ^0$C). The distance between the substrates and the evaporation source was around 0.20 m.

3.2 Substrates cleaning technique:

Initially the substrates were cleaned in chromic acid and then by ultrasonic. Then the substrates were suspended in the ultrasonic wave generator tank which contains detergent water and agitated with ultrasonic frequency. And lastly substrates were rinsed in distilled water and dried. Substrates are mounted on the substrate holder plate and kept in the vacuum chamber. Before deposition of the Ag films again all the substrates were cleaned by ionic bombardment technique in the vacuum chamber. Prior to deposition of the film, the system was thoroughly degassed. We could heat the film, in-situ, up to 160 ^{0}C at a rate of 5 ^{0}C /min.

3.3 Liquid nitrogen trap:

We maintained the pressure inside the chamber at around 3 x 10^{-6} Torr during TCR measurements, using the liquid nitrogen trap. Liquid nitrogen trap provides optimum performance for diffusion pump. Liquid nitrogen trap mounted above the diffusion pump reduces the back streaming of diffusion oil vapor and prevents oil vapors/molecules from diffusion pump entering into the system and this provides clean and ultimate vacuum in the chamber. Further, it improves the efficiency of the system and allows it to reach low ultimate pressure.

3.4 Measurement of resistance:

The resistance measurements have been performed in-situ with the standard four probe technique [16]. We have used a constant current source to maintain a current of 0.01 mA through the film. The temperature of the film was measured by a Chromel-Alumel thermocouple held rigidly very near to the substrate. TCR measurements were taken during heating and cooling cycles.

3.5 Sample preparation for SEM analysis:

The Ag films grown on different substrates were examined in a scanning electron microscope. A sample of suitable size was taken, grounded, polished and then etched using suitable etchant.

3.6 Sample preparation for EDS analysis:

Sample preparation for EDS analysis will be the same as that for SEM analysis.

4. Results and discussion:

4.1 Electron Mean Free Path(*l*) in bulk Ag:

From the equation (1), we obtained the electron mean free path in bulk Ag as 52.5 nm. Hence, we have selected the thickness range around the bulk mean free path, 50-150 nm [17,18].

4.2 Electrical resistivity of thin Ag films:

In Fig. 1, we have drawn the graph of electrical resistivity (ρ) against film thickness (t) for Ag films. The electrical resistivity is quite large for less thick films; resistivity decreases with increasing the film thickness and finally attains a constant value of about 4×10^{-8} Ω m after about a thickness of 80 nm.
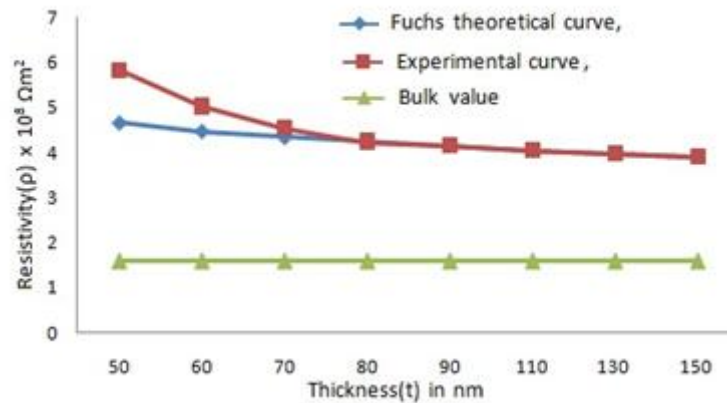
Fig. 1 Variation of electrical resistivity(ρ) with thicknesses(t) for Ag films.

In Fig. 2, we have shown the plot of ($\rho \times t$) versus (t) , based upon the Fuchs-Sondheimer in equation (2). The graph is found to be a straight line for the thickness range from 80-150 nm. The intercept of this plot on the axis ($\rho \times t$) yields the value of $\frac{3 \, \rho_0 \, l \, (1-p)}{8}$ and its slope gives the value of ρ_0, the resistivity of an infinitely thick Ag films. The values of ρ_0 and $l\,(1-p)$ obtained from this linear plot are 3.53×10^{-8} Ω m and 42.8 nm, respectively. Using these values of ρ_0 and $l\,(1-p)$ for total diffuse scattering (i.e. $p = 0$) , we have tried to fit our experimental data, using equation (4) by giving different values to p in the range 0 to 1. The best fit between our experimental data and Fuchs – Sondheimer   theoretical curve is obtained for $p = 0$. This value of p is then used to estimate the value of electron mean free path (l) , which comes out to be 42.8 nm.
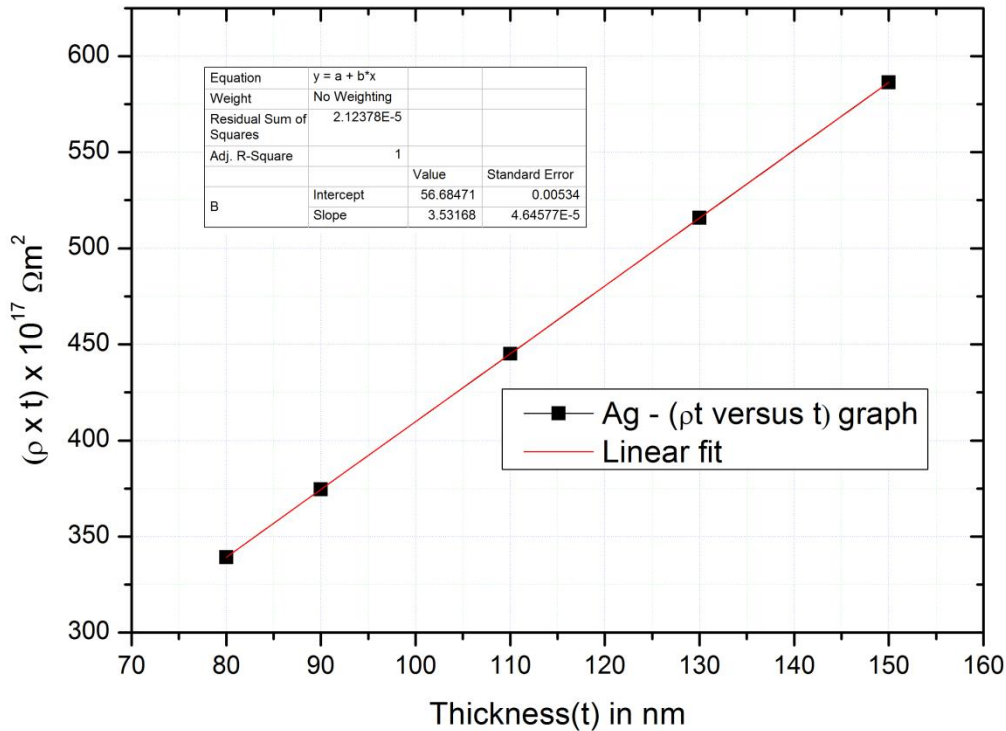
Fig. 2. Plot of (ρ x t) against (t) for Ag films of thicknessess, $t > l$

The film resistivity, ρ, versus thickness (t) experimental curve does not approach the bulk value ρ_B, 1.59 x 10^{-8} Ω m and 1.587 x 10^{-8} Ω m [19, 20], up to 150 nm thickness as shown in the Fig. 1. But we observed a saturation value of resistivity (ρ_s) about 4 x 10^{-8} Ω m after about a thickness 80 nm and found that the infinitely thick film resistivity of 3.53 x 10^{-8} Ω m. Both the resistivity are comparable (i.e. ρ_s & ρ_0). Although there is a good agreement between F-S theory and our experimental points of resistivity data for higher film thicknesses, there is a wide difference between Fuchs theoretical curve and our experimental data for lower thickness films. This is because F-S theory considers only size effects but disregards the scattering of electrons from grain boundaries. Similar type of deviation between the F-S and experimental curves for the resistivity data has been reported for other substances like palladium (Pd) [21], samarium (Sm) [22], manganese (Mn) [23], yttrium (Y) [24] , ytterbium (Yb) [25], nickel (Ni) [26], tin(Sn) [27] and vanadium (V) [28].

We tried to fit our experimental data with MS theory. The theoretical curve based on MS theory is denoted by the upper most curve in Fig. 1. It is clear that there is a good agreement between the MS theory and the experimental data for thinner films where grain boundary scattering is predominant. To calculate R', we assume the grain diameter, d, to be equal to the

thickness of the film i.e., 70 nm or below where the experimental data deviates from the FS theoretical curve. However, for higher thicknesses (>70 nm) the grain diameter becomes very large in comparison with the mean free path of electron conduction and hence contribution to the film resistivity from the grain boundaries become negligible. The difference between the resistivity from the F-S theoretical curve and the experimental data gives ($\frac{3\rho_0\alpha^{'}}{2}$).

Using the values of (ρ_0) and (l) estimated from the Fuchs theory, we obtained the value of $\alpha^{'}$ and from this the constant $R^{'}$ (average) is found to be 0.155, as shown in the Table 1. These are used in the equation (7) to obtain MS theoretical curve.

Table 1

Sl.no	Thickness(t), in nm	$\alpha^{'}$	$R^{'}$	$R^{'}$ (average)
1	50	0.1530	0.150	
2	60	0.0944	0.117	0.155
3	70	0.1510	0.198	

Although there is a good agreement between Fuchs theory and our experimental points of resistivity data for higher film thicknesses, there is a wide difference between Fuchs theoretical curve and our experimental data for lower thickness films. This is because Fuchs theory considers only size effect but disregards the scattering of electrons from grain boundaries. Similar type of deviation between the Fuchs and experimental curves for the resistivity data has been reported for other substances like Sm [22], Mn [23], Yb [25] , Ni [26] . Fuchs theory holds good to our experimental data for $p = 0$, indicating total diffuse scattering of conduction electrons in Ag films. From this value of p, we have calculated the electron mean free path, $l = 42.8$ nm, which is somewhat less than that reported for bulk value, 52.5 nm . It has been reported for many metallic films such as Sm [22], Mn [23], Yb [25], V [28], that the value of 'l' estimated from the resistivity data is higher than that estimated from the TCR data.

4.3 Temperature Coefficient of Resistance (TCR) of Ag films:

The TCR (α) measurements for Ag films have been carried out, in the temperature range between 26 - 150 ^{0}C. The TCR is found to be positive and thickness dependent. That is for lower thicknesses, the TCR has small positive value and increases as thickness increases, and finally attains a constant value of about 3.5 x $10^{-3}/\,^0$C after a thickness of about 80 nm, as shown in Fig. 3.
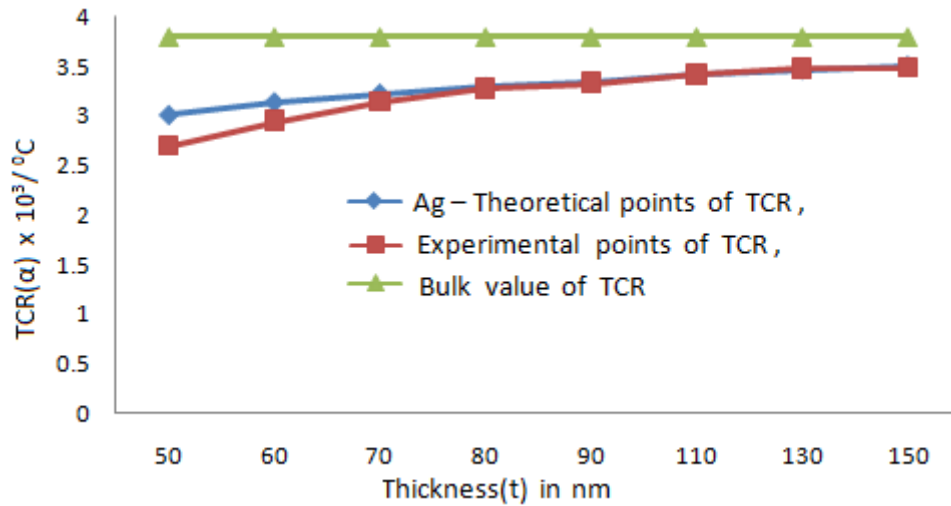
Fig. 3 Variation of temperature coefficient of resistance (α) with thickness (*t*) for Ag films.

Fig. 4 shows the plot of (α x *t)* against (*t*) based upon F-S equation (11) for TCR. This is found to be straight line with a slope (α_0) and an intercept on (α x t) axis as $\frac{3\ \alpha_0\ l\ (1-\ p)}{8}$, which have the values 3.73 x 10^{-3} / ^{0}C and 26.28 nm, respectively. A fairly good agreement is obtained between our experimental points and Fuchs theoretical curve for $p = 0$, for higher thicknesses. This value of *p* gives *l* as 26.28 nm. The TCR value obtained from our measurements is less than that of reported bulk value, 3.8 x 10^{-3} /^{0}C. The Fuchs equation for TCR curve fits to our experimental data for higher thicknesses range for $p = 0$, indicating total diffuse scattering.
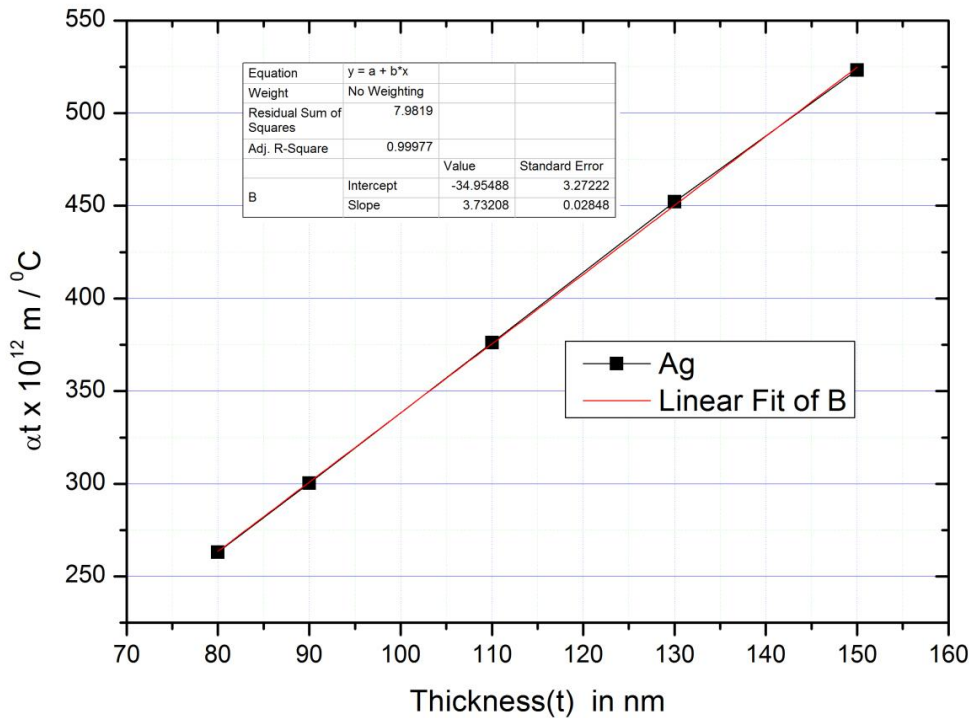
Fig. 4 Plot of $(\alpha \times t)$ against (t) for Ag films of thicknesses $t > l$

From our TCR and resistivity measurements on Ag films, it is found that $(\alpha \times \rho)$ = constant. This indicates that the Mathiessen's rule equation (10) is valid for Ag films. It has also been reported that Mathiessen's rule is valid for Ta [29], Ni [26], Pd [21] and Sm [22] films, since the TCR of Ag is positive and found to be a function of temperature (T).

F-S theory holds good to our experimental data for $p = 0$, indicating total diffuse scattering of conduction electrons in Ag films. From this value of p, we have calculated the electron mean free path, $l = 26.28$ nm, which is somewhat less than that reported for bulk, where it's value is 52.5 nm.

The value of electron mean free path calculated from our resistivity data (42.8 nm) is found to be more than that of TCR data (26.28 nm). It has also been reported for many metallic films such as Yb [25], Sm [22], Mn [23], the value of electron mean free path (l) estimated from the resistivity data is higher than that estimated from the temperature coefficient of resistance data.

4.4 Activation Energy(E_a) of Ag:

The plot of Ln R″ versus (1000 / T) for various thicknesses; 50 nm, 60 nm and 70 nm is shown in Fig. 5, based on equation (12) for Ag films.
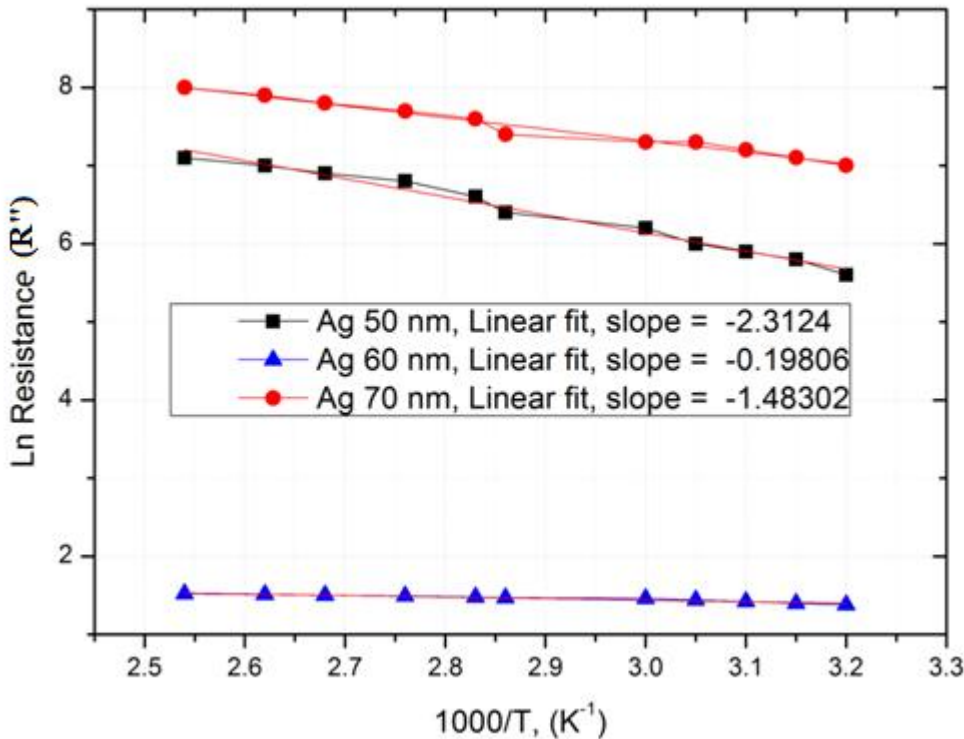

Fig. 5 Plot of Ln Resistance (R'') as a function of (1000 / T) for Ag films at various film thicknesses (*t*).

These straight lines have slope ($\frac{E_a}{K}$). The values of E_a obtained from these plots are in the range of 0.017 to 0.200 eV for Ag films, which are shown in Fig. 6.

Then we have plotted (E_a) against (*t*) graph (Fig. 6), which shows that activation energy decreases with the increasing film thickness. During the initial stages of growth of metallic films, a particle structure has been pointed out by many investigators [30, 31]. As the deposition of the metal continues, the particle size increases by accreditation and coalescence until the particles grow together to form a continuous film. In the case of Ag films, we observed that the activation energy decreases with increase in film thickness. This is attributed to increase of island dimensions with the increase of film thickness. The activation energies calculated for Ag films of thickness range from 50 nm to 70 nm varies from 0.017 to 0.200 eV. This type of behavior has also been observed in the case of tin [32] and in other metals.
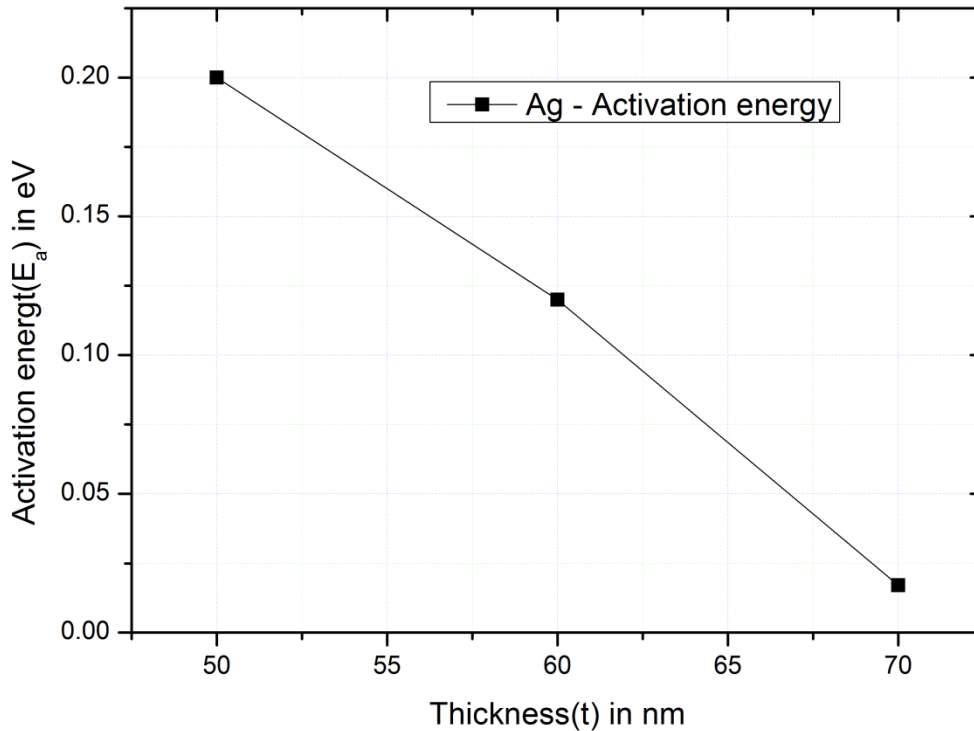
Fig. 6 Plot of activation energy(E_a) against thickness(t) for Ag films.

(4.5) Thickness dependence of microstructure and substrate materials in Ag thin films.

There are several stages in the growth process from initial nucleation to the final continuous three dimensional formation states. The microstructure of thin films is often dictated by the environment during the film formation, the nature of the thin film deposition, substrate material and film thickness. According to Walton [33] some critical nuclei are formed from vapor phase on condensation at the substrate, shown in the Fig. 7 (a), (b) & (c) for Ag films 10 nm thickness grown on glass, mica and teflon substrates, respectively under the same magnification.
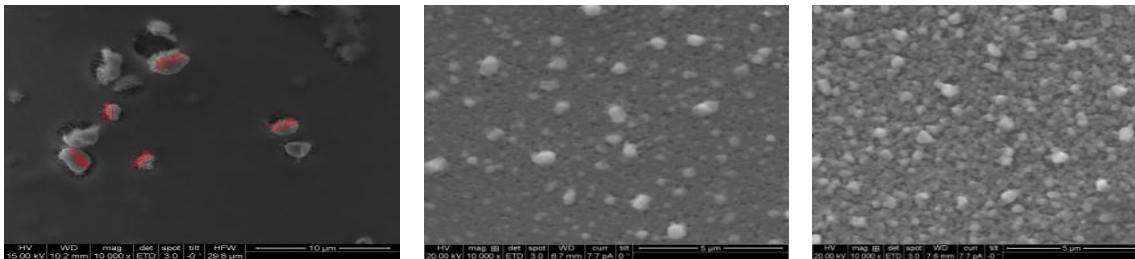
(a)   (b)   (c)

Fig. 7 SEM images of Ag films with thickness of 10 nm at 10,000x magnification for (a) Ag on glass, (b) Ag on mica and (c) Ag on teflon.

During the growth of thin films or the formation of dispersed deposits on substrates, these films tend to adopt some atomic arrangements depending on various factors interlay crystallographic structures of the deposit and of the substrate. The morphology and microstructure of vapor deposited thin Ag films has been studied by many researchers [34, 35]. The nucleation, growth and metastable-to-stable phase transformation behavior of Ag thin films were studied by means of Scanning Electron Microscopy (SEM), but most of the individual island remain as crystalline units or grains distinct separated by grain boundaries with transition regions of several atomic layers thick between differently oriented crystalline units. At any constant temperature the grain size increases with thickness. But in the case of samples of the compound of the single Perovskite $La_{0.67}Ca_{0.33}MnO_3$, the grain size increases with temperature as noticed by Mohammed *et al*. [36]. The results confirm that nucleation begins at the surface of the film and proceeds by the growth of grains as shown in Fig. 7 (a), (b) and (c).

As the thickness increases to 20 nm the grain size also increases, which has been shown in Fig. 8 (a), (b) and (c). There is interconnection of islands and hence a quasi-contiuous structure is formed. The structure mainly depends on the substrate material and the binding force between substrate material and Ag deposited.
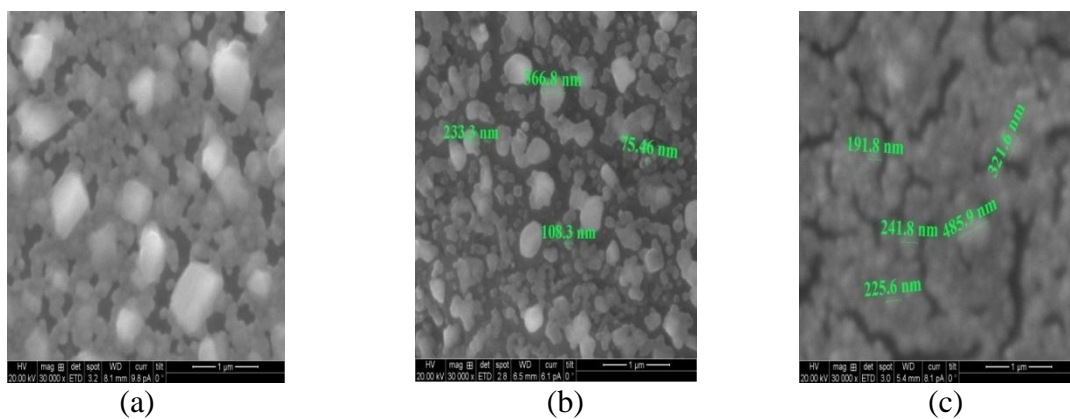

(a)　　　　　　　　　　(b)　　　　　　　　　　(c)

Fig. 8 SEM images of Ag films of 20 nm thick at 30,000x magnification for (a) Ag on glass, (b) Ag on mica and (c) Ag on teflon.

As the thickness increases further the grains grow in bigger size and elongated grain shape as shown in Fig. 9 (a), (b) and (c), due to coalescence.

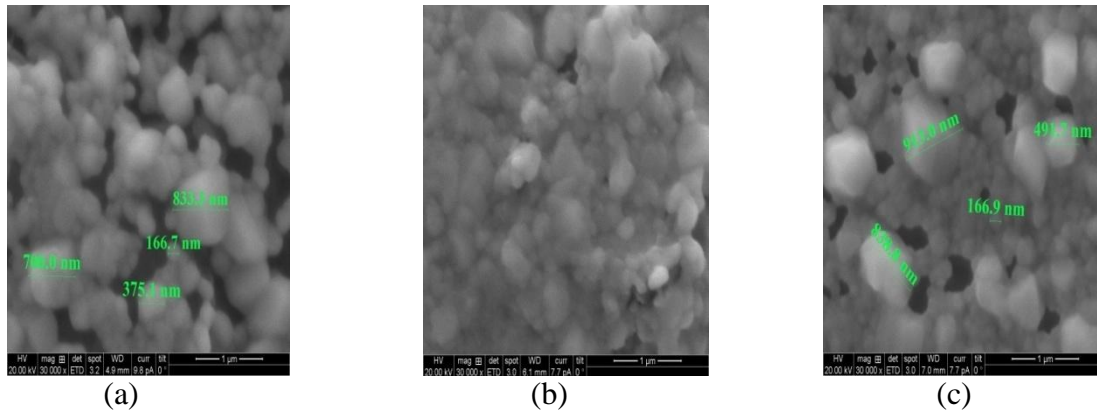(a)   (b)   (c)

Fig. 9 SEM images of Ag films of 65 nm thick at 30,000x magnification for (a) Ag on glass, (b) Ag on mica and (c) Ag on teflon.

It is found that higher island sizes are formed as thickness of the film is increased. The islands as they grow, developed some characteristic shapes and then with further growth coalescence with the neighboring one by rounding off their edges near joining regions. The coalescence involves considerable transfer of mass between islands by diffusion. Small islands disappear rapidly. During coalescence of two islands re-crystallization takes place leading to some definite shapes of larger islands [30,35].

It is observed from the Figs, 7, 8 and 9 that the structure of the film depends on substrate material, substrate roughness/smoothnes and the sticking coefficient between the substrate material and Ag films. Moreover, the substrate material happens to be one of the deposition parameters, which regulates the morphology and microstructure of Ag films. We get different structures when Ag films are coated on glass, mica and teflon substrates for the same magnification and thickness indicating the binding forces are different. It is visible that the particles are different in size when coated on different substrates for the same thickness as evidenced by the Fig. 9 (a), (b) and (c).

4.6 Energy Dispersive Spectroscopy, EDS Analysis:

It relies on the investigation of a sample through interactions between electromagnetic radiation and matter, analyzing x-rays emitted by the matter in response to being hit with charged particles. Its characterization capabilities are due in large part to the fundamental principle that each element has a unique atomic structure allowing a unique set of peaks on its electromagnetic emission. Fig.10 shows the EDS spectrum of Ag, displays the characteristic prominent peak indicating that the material utilized in the present investigation is Ag, since the Ag films are deposited on glass substrates. It is noticed in the same figure that the peaks occur at the energies of 3.2 and 3.3 eV and the other peaks corresponds to the chemical contents of the glass substrate.

In the case of nickel substituted in cadmium ferrite, prominent peaks were observed by Chavan et al, 2013 [37] while checking the purity and the chemical composition of the elements using energy dispersive X-ray (EDX) spectrograph. The elemental composition of

CdS thin films analyzed using EDS reveals peaks corresponding to cadmium and sulphur with appreciable intensity of cadmium peak and sulphur peak have been noticed by Pushpalata *et al*., 2014 [38].
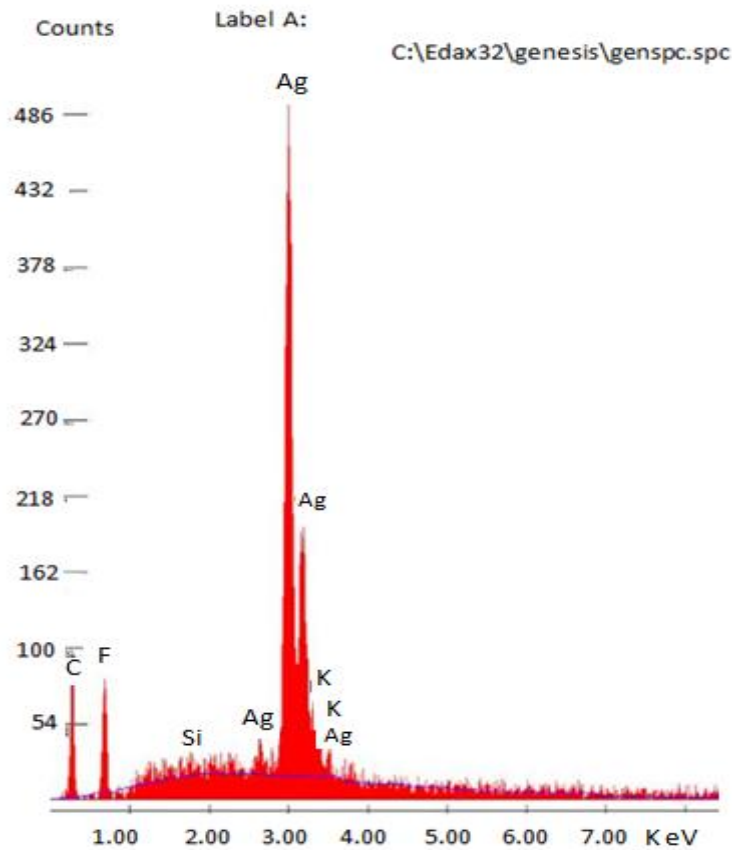

Fig. 10. The EDS spectrum of a 65 nm thick of Ag with x-axis is the energy level and y-axis is the counts (number of X-rays received and processed by the detector).

5. Conclusion :

The electrical and microstructural response of Ag films approaching the thickness in the range of electron mean free path and more thickness were studied theoretically as well as experimentally. The response of the thickness on the microstructure and electrical properties of Ag thin films is presented.

In very thin films, major portion of the resistivity arises due to the scattering of the electrons at the grain boundaries, in addition to the isotropic background scattering due to the external surfaces. If we take into consideration all these scattering mechanisms, the experimental resistivity data for Ag films will closely fit with the Mayadas – Shatkzes theory for the entire range of film thickness. As we ignored the scattering of grain boundaries, a wide difference in the theoretical and experimental curves is seen, particularly, in the lower thickness region for Ag films. Mathiessen's rule holds good for Ag films because of its positive TCR.

The values of electron mean free path estimated for Ag films by the measurement of resistivity and TCR are comparable with that of bulk value. Similarly the specularity parameter (p) used for fitting the experimental data with the theoretical curve is found to be the same, for both resistivity and TCR data. The infinitely thick film resistivity and TCR for Ag films are of the same order of magnitude of the bulk Ag, respectively. We observe that, the activation energy for Ag films decreases with film thickness, as in the case of other metals.

Detailed observation has been made on the microstructure of thermally evaporated Ag films. There are several stages in the growth process from initial nucleation of the deposits to the final continuous three dimensional state. The stages of the film growth have been observed by scanning electron microscopic (SEM) studies. From the knowledge of the initial stages of growth one can interpret that whether the film helps in the conduction of current or not and suitable for AC/ DC conduction mechanism. Further, the EDS analysis study confirms that the material under investigation is Ag.

Acknowledgement :

References :

[1] Monsieur H. A., *Projet Cocotrans*, (2011) Project ID: Anr-11-Rmnp-0010.

[2] Guowen D., Cesar C., Daniel S., Minh L., *AIP Advances*, **5** (2015) 117234.

[3] Bouhafs D., Moussi A., Chikouche A., Ruiz J. M., *Solar Energy Materials and Solar Cells*, **52** (1998) 79.

[4] Xu. J., Shun Y., Pan Q., Qin J., *Sensors and Actuators*, **B66** (2000) 161.

[5] Yang L., Zhang T., Zhou H., Price S. C., Wiley B. J., You W., *American Chemistry Society Applied Material and Interfaces*, **3** (2011) 4075.

[6] Zakia F., Nazir M., Ali H., *American Journal of Modern Physics*, **3**, (2014) .45.

[7] Drachev V. P., Nashine V., Thoreson M. D., Khaliullin E. N., Ben-Amotz D., Davisson V. J., Shalaev V. M., *Lasers and Electro-Optics Society*. (2004) The 17th Annual Meeting of the IEEE, DOI: 10.1109/LEOS.2004.1363298.

[8] Charles K., "*Introduction to Solid State Physics*", Wiley India Pvt. Ltd., Seventh Edition, (2010) 158.

[9] Larson D., " *Physics of thin films*'', Edited by Francombe M. H., Hoffman R. W., Academic Press, New York, (1970) 84.

[10] Sondheimer E. H., *Advances in Physics,* **1** (1952) 1.

[11] Mayadas A. F., Shatzkes M., *Physical Review* B, **1** (1970) 1382.

[12] Horvath G., Bankuti J., *Physica Status Solidi (a),* **110** (1988) 549.

[13] Gould G. N., Moraga L. A., *Thin Solid Films*, **10** (1972) .327.

[14] Ekertova L., *"Physics of thin films''*, Plennm Press, New York, (1977) 168.

[15] Goswami A., *"Thin Film Fundamentals''*, New Age International (P) Limited Publishers, (1996) 245.

[16] Thakur M. K., Singh O. P., Thakur K., Gaur K. S., Muhanthan N., Singh S., Singh D., Vijayan N., Singh H. K., Singh V. N., *Advanced Materials letters*, **7** (2016) 525.

[17] Shiva L. U., Ayachit N. H., Udachan L. A., Banagar A. V., Kolkundi S. S., Bhairamadagi S. S., *Bulgarian Journal of Physics,* **45** (2018) 35.

[18] Vyas S. M., Patel M., Thakor S., Patel V., Patel P., *International Journal of Latest Technology in Engineering, Management & Applied Science*, III (2014) 166.

[19] *"Hand Book of Physics and Chemistry''*, Chemical Rubber Company Press, Cleveland, Ohio, 54th edition, (1974) F155.

[20] Daniel G, *Journal of Applied Sciences*, **119** (2016) 085101.

[21] .Shivaprasad S. M, Udachan L. A, Angadi M. A, *Physics letters*, **78A** (1980) 87.

[22] Ashrit P. V, Angadi M. A, *Journal of Less-Common Metals*, **72** (1980) 317.

[23] Shivaprasad S. M, Ashrit P. V, Angadi M. A, *Physica Status Solidi (a)*, **60** (1980) K159.

[24] Ashrit P. V, Shivaprasad S. M, Angadi M. A, *Thin Solid Films*, **72** (1980) L5.

[25] Ashrit P. V, Angadi M. A, *Physica Status Solidi (a)*, **63** (1981) K77.

[26] . Angadi M. A . Udachan, L. A, *Thin Solid Films* , **79** (1981) 149.

[27] Angadi M. A, Udachan L. A, *Thin Solid Films*, **78** (1981) 299.

[28] Chander R, *Physica Status Solidi (a)*, **14** (1972), K31.

[29] Altman C, *Proceedings Nineeth National Vacuum Symposium*, (1962) 174.

[30] Mohd Abdul M. K, Sushil K, Maqusood A, Salman A. A. Mohammad S. A, , *Nanoscale research letters,* **6** (2011), 434.

[31] Andressa C. S, Marcelo B. P, Flavio H, Raquel S. M, Carla R. M, Manuela P. K, Flinho F. H, Tania M. H. C, Eliana W. D. M, Edilson V. B, *Journal Of Brazilian Chemical Society,* **26** (2015) 1004.

[32] Udachan L. A, Jogad M. S, Rama Rao S, *Asian Journal of Physics* **8** (1999) 207.

[33] Walton D, *Journal. Of Chemical. Physics.* **3** (1962) 2182.

[34] Muhammad M, Tahirzeb K, *Surface Review and Letters.* **12** (2005) 759.

[35] Dimitrijević R, Cvetković O, Miodragović Z, Simić M, Manojlović D, Jovic V, *Journal of Mineral Metallurgy Section B-Metal,* **49** (2013) B91.

[36] Mohammed I. M, Elbadawi A. A, Abuellhassan H. H, *Journal of Applied and Industrial Science,* **1** (2013) 12.

[37] Chavan G. N, Papanna B, Naik L. R, Sunil Kumar, *International Journal of Science and Technology Research*, **2** (2013) 82.

[38] Pushpalatha H. L, Bellappa S, Narayanaswamy T. N, Ganesha R, *Indian. Journal. Of Pure and Applied. Physics.* **52** (2014) 545.